# Correlations between the structure and dielectric properties of $Pb(Sc_{2/3}W_{1/3})O_3-Pb(Ti/Zr)O_3$ relaxors

Pavol Juhas*
*Department of Physics and Astronomy, Michigan State University, East Lansing, Michigan 48824, USA*

Ilya Grinberg and Andrew M. Rappe
*The Makineni Theoretical Laboratories, Department of Chemistry, University of Pennsylvania, Philadelphia, Pennsylvania 19104-6323, USA*

Wojtek Dmowski
*Department of Materials Science and Engineering, University of Tennessee, Knoxville, Tennessee 37996, USA*

Takeshi Egami
*Oak Ridge National Laboratory, Oak Ridge, Tennessee 37831, USA*
*and Department of Materials Science and Engineering and Department of Physics and Astronomy, University of Tennessee, Tennessee 37996, USA*

Peter K. Davies†
*Department of Materials Science and Engineering, University of Pennsylvania, Philadelphia, Pennsylvania 19104-6272, USA*
(Received 2 February 2004; published 4 June 2004)

Solid solutions of $(1-x)Pb(Sc_{2/3}W_{1/3})O_3-(x)PbTiO_3$ and $(1-x)Pb(Sc_{2/3}W_{1/3})O_3-(x)PbZrO_3$ (PSW-PT and PSW-PZ) show remarkably different dielectric responses. Even though PT has a much higher Curie temperature (490 °C) than PZ (230 °C), addition of Ti up to $x\approx0.25$ decreases $T_{\epsilon,\max}$ — in contrast to the increase of $T_{\epsilon,\max}$ for the substitution of PZ. Concentrations of Ti with $x>0.25$ lead to a strong increase in $T_{\epsilon,\max}$. The structural origins of this behavior were studied by x-ray and neutron diffraction, pair distribution function (PDF) analysis and density functional theory (DFT) calculations. For $x<0.25$ the B cations form a 1:1 ordered doubled perovskite structure (space group $Fm\bar{3}m$) in agreement with the ''random site model,'' where the ordered structure consists of one B sublattice occupied by Sc and the other by a random mixture of the remaining cations. The B site order is reduced by incorporation of Zr, but highly stabilized by Ti with the degree of order in excess of 95% for $x\leqslant0.25$. The results of PDF analysis and DFT calculations show that locally the atoms are significantly displaced from their average lattice positions and that $T_{\epsilon,\max}$ is strongly correlated with the cation displacements. The initial anomalous decrease of $T_{\epsilon,\max}$ in PSW-PT is due to the suppression of ferroelectricity by a decrease in the perovskite volume and is related to reduced Pb displacements. For $x<0.25$ the contribution to ferroelectric polarization from Ti and W are restricted because of the high B-site ordering. However, as the order is reduced for $x>0.25$, the active Ti and W cations couple their displacements and dominate the dielectric response, driving $T_{\epsilon,\max}$ up. For PZ substitution, the lack of ordering leads to nearly linear growth of $T_{\epsilon,\max}$ corresponding to a uniform increase in Pb and B-cation displacements.

DOI: 10.1103/PhysRevB.69.214101 PACS number(s): 77.84.Dy, 71.15.Mb, 61.66.Fn

## I. INTRODUCTION

Lead-based $PbBO_3$ systems in the perovskite structure can accommodate mixing of several cations on the B site, allowing the formation of many compounds and their solid solutions with a variety of dielectric and piezoelectric properties controlled by the chemistry at the B site. The B-site arrangement can be macroscopically described by the composition and distribution of the cations on the B sublattice. Modification of either of these parameters can induce a significant changes in the dielectric response. For example, for different B compositions lead-based perovskites can exhibit ferroelectric ($PbTiO_3$), antiferroelectric ($PbZrO_3$), or relaxor-type [$Pb(Mg_{1/3}Nb_{2/3})O_3$] behavior. Every lead-based system with a relaxor response has a mixture of different cations on the B site, and this appears to be a necessary condition for the relaxor behavior. A change in the ordering of the B site can also induce changes in dielectric response. One well-known example is the $Pb(Sc_{1/2}Ta_{1/2})O_3$ (PST) system, where the chemical ordering of $Sc^{3+}$ and $Ta^{5+}$ induces a transition from relaxor to normal ferroelectric behavior and an increase in the paraelectric transformation temperature. In ordered PST, the $Sc^{3+}$ and $Ta^{5+}$ cations form a rock-salt structure, with a doubled unit cell and 1:1 alternation of Sc and Ta planes along the $\langle111\rangle$ directions. In fact, all ordered Pb-based mixed metal perovskites adopt this 1:1 ''double perovskite'' structure [$Pb(\beta'_{1/2}\beta''_{1/2})O_3$], even compounds with 2:1 or 1:2 B-site cation stoichiometries. The $Pb(Mg_{1/3}Nb_{2/3})O_3$ (PMN) type compounds are the best known example of such incompatibility between the cation stoichiometry and the symmetry of the resultant ordered structure. A series of recent studies of tantalate [$Pb(Mg_{1/3}Ta_{2/3})O_3$ — PMT] and niobate members of the PMN family have showed this incompatibility is accommo-

 

dated through the formation of a ''random site'' structure where one position is occupied solely by Nb (or Ta), and the other contains a random mixture of Mg and the remaining Nb/Ta cations.[1–4] Although the ordered lead-based perovskites have similar 1:1 structures, the effects of order on the dielectric properties are highly nonuniform. For example, in $Pb(Sc_{1/2}Nb_{1/2})O_3$ (PSN) the increase in B-site order causes relaxor-type broadening of the paraelectric transition and a significant decrease of the transition temperature.[5–7] This is just the opposite to the behavior of the related PST system,[8–10] even though PSN and PST might be expected to have similar properties. On the other hand, for the $(0.95)Pb(Mg_{1/3}Ta_{2/3})O_3-(0.05)PbZrO_3$ system, an increase of the B-site order from 20% to 95% did not induce any appreciable change in dielectric properties.[1]

Although the B-site chemistry is critical for the overall dielectric response of lead-based perovskites, a significant part of the polarization comes from the off-centering of the A-site Pb ions, which has been reported for numerous systems.[11–14] The $Pb^{2+}$ cations have a ''lone pair'' electron configuration with two electrons outside the closed *d* shell. The outer electrons form a lone-pair orbital on one side of the atom, which induces a displacement of the lead and formation of short Pb-O bonds. These displacements are thus controlled by the local environments of individual Pb atoms, in particular by its oxygen neighbors. The Pb-O bonds are also influenced by the bonding of oxygen to its nearest B-site neighbors, and as a result the oxygen anions mediate the interaction between the Pb displacements and the B-site chemistry. The exact relationship between the macroscopic dielectric properties and the B-site structure is complicated and driven by many coupled interactions. In this paper, we investigate these relations in $Pb(Sc_{2/3}W_{1/3})O_3-PbTiO_3$ and $Pb(Sc_{2/3}W_{1/3})O_3-PbZrO_3$ solid solutions.

These systems are ideally suited for such a study, as they show completely different responses to the B-site substitution in spite of their similar chemistries. PSW is similar in properties to the PMN family of compounds, since it displays a relaxor-type response and also forms a B-site ordered structure with 1:1 periodicity. The effects of cation substitutions and thermal treatments on the B-site order and dielectric properties in $(1-x)Pb(Sc_{2/3}W_{1/3})O_3-(x)PbTiO_3$ (PSW-PT) and $(1-x)Pb(Sc_{2/3}W_{1/3})O_3-(x)PbZrO_3$ (PSW-PZ) have been previously reported elsewhere.[15] It was found that the amount of order in the PSW-PT system can be controlled by the synthesis conditions and that similar to PSN, an increase in B-site order leads to a significant decrease in the transition temperature. The results indicated that the 1:1 order in PSW can be represented by a modified ''random site'' structure. According to this model, the structure of the fully ordered PSW end member can be represented as $Pb[Sc]_{1/2}[Sc_{1/3}W_{2/3}]_{1/2}O_3$ and the ordered solid solutions by $Pb[Sc]_{1/2}[Sc_{(1-4x)/3}W_{(2-2x)/3}M^{4+}_{2x}]_{1/2}O_3$, where $M^{4+}$ is either Ti or Zr. Because of the $(1-4x)/3$ term, this substitution pattern for the solid solutions is only possible for $x \leqslant 0.25$. For $x > 0.25$ the $M^{4+}$ cation must substitute on both lattice sites, to give stoichiometries with $Pb[Sc_{(4-4x)/3}M^{4+}_{(4x-1)/3}]_{1/2}[W_{(2-2x)/3}M^{4+}_{(2x+1)/3}]_{1/2}O_3$.

The order parameter of PSW-PT and PSW-PZ samples has been evaluated from conventional powder x-ray diffraction (XRD) by comparing the measured intensity of the (111) superreflection ($d \approx 4.7$ Å) to its calculated value, see Fig. 1. For PSW-PT the cation order was found to be much more stable and extend to higher substitution levels than for its PSW-PZ counterpart. This observation could be interpreted in terms of the difference of the average cationic size for $\beta'$ and $\beta''$ sublattices predicted by the random site model ($r_{Sc^{3+}} = 0.745$ Å, $r_{W^{6+}} = 0.60$ Å, $r_{Ti^{4+}} = 0.605$ Å, and $r_{Zr^{4+}} = 0.72$ Å, in pure PSW $r_{\beta'} = 0.745$ Å and $r_{\beta''} = 0.65$ Å). The size difference $(r_{\beta'} - r_{\beta''})$ increases with *x* for the Ti system (since $r_{Ti^{4+}} < r_{\beta''}$), but decreases for the substitution of Zr.

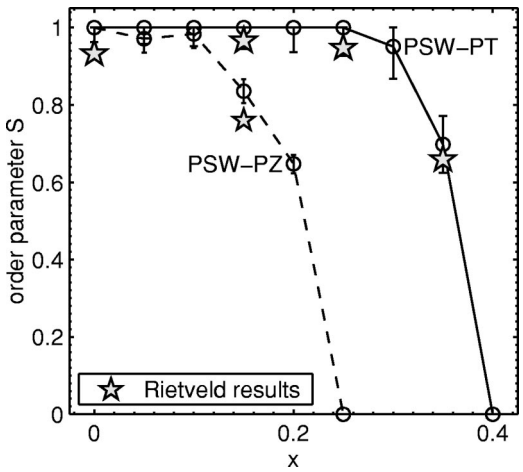


FIG. 1. Degree of order *S* as a function of composition *x* for PSW-PZ and PSW-PT. Circles mark data from conventional XRD, stars mark results of Rietveld analysis of the synchrotron XRD.

All of the investigated compositions show relaxor ferroelectric behavior; however PSW-PT displays an unusual trend in the temperature of the permittivity maximum $T_{\epsilon,\max}$, which decreases for $x \leqslant 0.2$ and then increases for $x > 0.25$. In contrast, for the PZ system $T_{\epsilon,\max}$ varies linearly with the Zr content, as displayed in Fig. 2. These observations can be rationalized in terms of the B-site occupancies predicted by

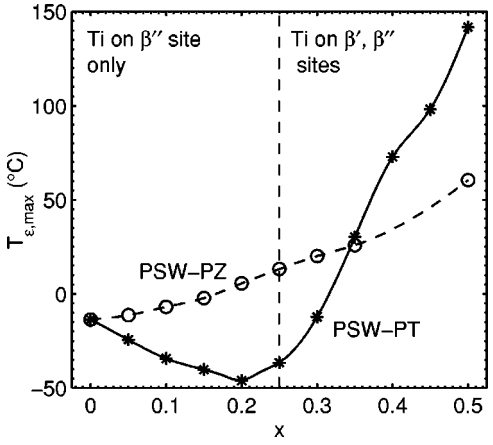


FIG. 2. Variation of $T_{\epsilon,\max}$ (1 MHz) with *x* for PSW-PT and PSW-PZ. PSW-PT solution shows a surprising drop in $T_{\epsilon,\max}$ for $x \leqslant 0.2$.

the random site model. For the substitution of PT complete order occurs for $x \leqslant 0.25$ (Fig. 1), therefore one lattice site is occupied exclusively by Sc and the other by a mixture of Sc, W, and Ti. However for $x > 0.25$ Ti must substitute on both ordered sites and the presence of Ti-O-Ti or Ti-O-W bonds becomes likely. It is precisely at this composition where the sharp growth in $T_{\epsilon,\max}$ is observed, see Fig. 2. The appearance of Ti-O-Ti and Ti-O-W neighbors can be responsible for longer range coupling of the ferroelectrically active $Ti^{4+}$ and $W^{6+}$ cations. It is also possible that the stronger bonding of oxygens in Ti-O-W and Ti-O-Ti chains may significantly alter the magnitudes and directions of Pb displacements. In the PSW-PZ system, the degree of order is less than 100% even for low substitution levels, implying that both ordered sites contain a mixture of several cations. Consequently there is no abrupt change in the pattern of B-site occupation and the linear behavior of $T_{\epsilon,\max}$ versus $x$ is not unexpected. Our previous data strongly supported the random site model as a correct description of the ordered PSW-PT and PSW-PZ compounds. Nevertheless more detailed structure analysis was necessary to determine the exact occupancies in the ordered phases and to probe the modifications in the atomic displacements that accompany the changes in composition, order, and dielectric response. Therefore we performed a detailed Rietveld and pair distribution studies of the PSW-PZ and PSW-PT systems using synchrotron x-ray (SXRD) and neutron diffraction (ND). We also modeled these solid solutions using density-functional theory calculations.

## II. EXPERIMENTAL PROCEDURES

### A. Sample preparation

The diffraction measurements were conducted on four samples of $(1-x)$PSW–$(x)$PT with $x=0$, 0.15, 0.25, and 0.35, and two solid solutions of PSW-PZ with $x=0.15$ and 0.35. These PSW-PT systems were chosen to probe the compositional range that displays the largest changes in the $T_{\epsilon,\max}$ behavior, Fig. 2. For comparison similar compositions were examined for PSW-PZ system. The samples were prepared by solid-state methods from high-purity oxides ($>99.9\%$) via the ''columbite route.'' Stoichiometric amounts of $Sc_2O_3$, $WO_3$, and $ZrO_2$ or $TiO_2$ powders were mixed in an agate mortar and calcined overnight at 1100 °C. PbO was then added to the mixture, which was ball milled and annealed for 6 h at 875 °C. This treatment resulted in the formation of a single phase powder, which was ball milled for 6 h and isostatically pressed (at 500 MPa) into pellets with diameters of 8 mm or 20 mm. The final sintering was done in a way known to maximize the B-site order. The pellets were annealed at temperatures between 910 °C–1050 °C, for durations of 6 h–24 h and slowly cooled at the rate of 1 °C/min. During these treatments the specimens were buried in a sacrificial powder of the same composition and wrapped in Pt foil to avoid second phase products from the loss of PbO. To further stabilize the perovskite phase, the wrapped samples were placed inside a tightly closed crucible with a $(0.1)$PbO–$(0.9)PbZrO_3$ spacer powder which provided a Pb-rich atmosphere. The phase purity, lattice parameters, and degree of ordering were checked using conventional powder XRD.

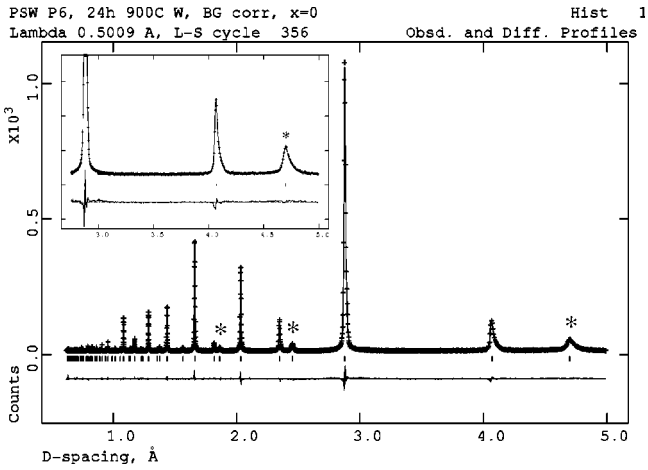


FIG. 3. Rietveld refinement of the PSW SXRD pattern. Crosses denote the experimental data, asterisks highlight the ordering reflections, and the difference curve is marked at the bottom part of the plot.

### B. Synchrotron X-ray diffraction

Synchrotron x-ray diffraction data were taken at the X7A beamline at the National Synchrotron Light Source, Brookhaven National Laboratory. Powder samples were placed in glass capillaries with a 0.1 mm diameter. Packing densities were found to be 5 g/cm$^3$–6.5 g/cm$^3$ (60%–80%) indicating a strong x-ray absorption (absorption length $\sim 0.05$ mm). During the measurement, the capillaries were rotated in order to improve orientational averaging. A low wavelength of $\lambda = 0.500\ 95$ Å, which reduced absorption by the Pb atoms, was selected with a Ge (111) monochromator. Diffraction intensities were measured using a position sensitive detector (PSD) with a 4° angular range and 0.3 mm $\times 10$ mm receiving slit. The diffraction data were collected in the $Q$ range of 1.1 Å$^{-1}$–10 Å$^{-1}$ ($d=0.62$ Å–5.8 Å) and analyzed by Rietveld method using the GSAS software package.[16] The x-ray background was subtracted using a cubic smoothing spline, and the measured intensities were corrected for absorption via the built-in GSAS procedure. The reflections were fitted by an asymmetric peak profile function 3, which is suitable for the setup with PSD detector. Peaks in the measured spectrum displayed considerable asymmetry (Fig. 3), which could be fitted by refining the $S/L$ parameter (beam aperture) in the profile function. The ordering reflections had wider profiles, because of the smaller size of the ordered regions. This could be modeled using the GSAS procedure for stacking fault broadening, which introduced separate broadening terms for the superlattice reflections. The x-ray wavelength and zero correction were determined by refinement of $CeO_2$ standard. The scale factor, background, lattice constant, peak profiles, temperature factors, oxygen positions, and B-cation occupancies were all refined.

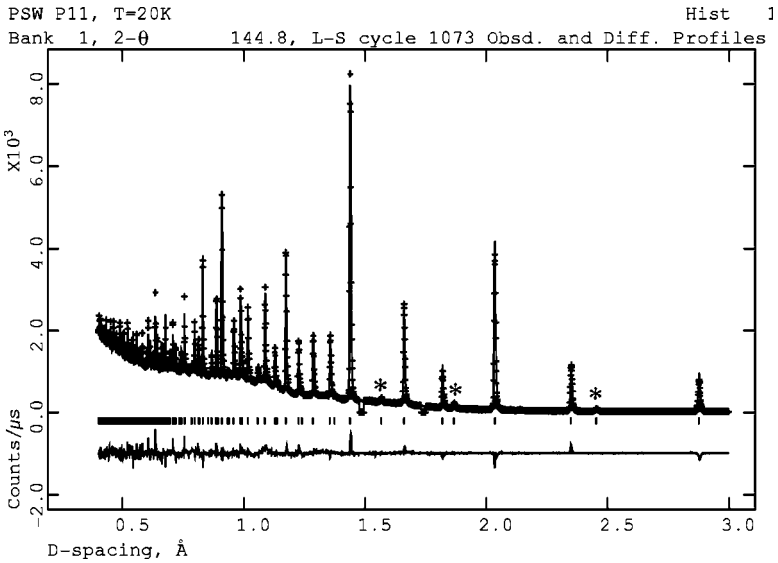


FIG. 4. Rietveld analysis of the ND data from PSW at 290 K. Crosses denote the experimental data, asterisks indicate ordering reflections, and the fit difference is marked at the bottom.

### C. Neutron diffraction

Time-of-flight (TOF) neutron-diffraction data were collected at the Special Environment Powder Diffractometer beamline at the Intense Pulse Neutron Source, Argonne National Laboratory. The specimens were placed in a cylindrical (11 mm in diameter) vanadium container, which was sealed under He atmosphere to ensure good thermal contact. The container was mounted on a He cooled displex cryostat and for all samples the diffraction data were measured for 5 h at 20 K and 290 K, below and above the paraelectric transition. The first, room-temperature run was carried out to check for any structural changes due to the cooling to low temperature. The incident neutron spectrum and scattering effects from the sample chamber were evaluated from calibration runs with the vanadium rod, empty displex, and displex with empty container. The ND data were evaluated by the Rietveld and pair distribution function (PDF) analysis. The Rietveld refinement was carried out using data from the 144.85° detector bank in the $Q$-range of 1.88 $Å^{-1}$–15.7 $Å^{-1}$ ($d$ range 0.4 Å–3.35 Å). No appreciable changes were observed in the results after a trial analysis using two detector banks at 90° and 144.85°. A Ni standard sample was used to evaluate the diffractometer constants. The absorption of neutrons was found to be negligible (absorption length $\sim$100 mm). The intensity background was modeled by a shifted Chebyshev polynomial, GSAS function 1, and the intensity peaks were refined using the GSAS TOF profile function 3. As for the SXRD, the additional broadening of the ordering reflections was facilitated by utilizing the stacking fault model for the {200} superlattice. The lattice parameter, background function, profile coefficients, B-site occupancies, temperature factors, and oxygen positions were all refined together. For the PDF analysis, the scattering intensities were regrouped to five detector banks at 21.8°, 44.0°, 90.0°, 139.7°, and 150.0°, which allowed good intensity resolution in the $Q$ range of 1.2 $Å^{-1}$–30 $Å^{-1}$. The PDFGETN software was used to correct the raw intensities for background and environment effects and to calculate the PDF.[17] The cutoff parameter, $Q_{max}=26$ $Å^{-1}$, for the Fourier transformation was chosen such that the differential change in the PDF curve with $Q_{max}$ would be minimal in the interval of 1.7 Å$<r<$10 Å. The simulations of the PDF curves were performed using the PDFFIT package.[18]

## III. RESULTS

### A. Rietveld refinements

The refined SXRD pattern of PSW obtained by the Rietveld method is displayed in Fig. 3, and the analogous neutron-scattering result at 290 K is presented in Fig. 4. The ordering reflections ($d\approx4.7$ Å) were observed in all samples (PSW-PT, $x=0.0$, 0.15, 0.25, 0.35 and PSW-PZ, $x=0.15$) with the exception of PSW-PZ, $x=0.35$. There was no sign of peak splitting in any of the measured x-ray or neutron spectra at 20 K or 290 K and all diffraction patterns were consistent with a cubic perovskite structure. No difference could be found between the neutron data measured before and after low-temperature cooling and there was no evidence for spontaneous polarization. The samples displaying B-site order were refined using the double perovskite structure, space group $Fm\bar{3}m$ (225). A simple perovskite lattice, space group $Pm\bar{3}m$ (221) was used for the disordered (0.65)PSW-(0.35)PZ system.

The total occupancies of all lattice sites were fixed to 1 and the occupancies of the B cations were required to satisfy the overall stoichiometry. For three different B cations these conditions permit two free parameters for the B site occupation, since specifying the populations of two B cations on $\beta'$ site automatically determines their content on the $\beta''$ site and the $\beta'$ and $\beta''$ populations for the third B-cation. However, only one of these parameters can be refined, because the structure factors of ordering reflections are proportional to the same value ($F_{ord}=4f_{\beta'}-4f_{\beta''}$). Therefore, the B occupancies were set to linearly change with a single parameter $S$, from a completely random structure ($S=0$) to the one with maximum order at $S=1$. The refined B occupancies and

TABLE I. B-site cation occupancies in PSW-PT and PSW-PZ vs order parameter $S$ for linear interpolation from completely random to completely ordered structure.

| | $x \leqslant 0.25$ | | $x > 0.25$ | |
|---|---|---|---|---|
| Cation | $\beta'$ | $\beta''$ | $\beta'$ | $\beta''$ |
| Sc | $\frac{2-2x}{3}+\frac{2x+1}{3}S$ | $\frac{2-2x}{3}-\frac{2x+1}{3}S$ | $\frac{2-2x}{3}(1+S)$ | $\frac{2-2x}{3}(1-S)$ |
| W | $\frac{1-x}{3}(1-S)$ | $\frac{1-x}{3}(1+S)$ | $\frac{1-x}{3}(1-S)$ | $\frac{1-x}{3}(1+S)$ |
| $Ti^{4+}$ or $Zr^{4+}$ | $x(1-S)$ | $x(1+S)$ | $x-\frac{1-x}{3}S$ | $x+\frac{1-x}{3}S$ |

their dependence on the order parameter $S$ are listed in Table I. The oxygen positions were refined in accordance with the $Fm\bar{3}m$ symmetry, which allows shifts along the $\beta'$-O-$\beta''$ bonds. Because of the limited $Q$ range, the SXRD data were simulated using isotropic temperature factors which had the same value for all B cations. In the case of the neutron spectra, which have a wider $Q$ range, the temperature factors for O were refined as anisotropic with components perpendicular ($U_{O11}$) and parallel ($U_{O33}$) to $\beta'$-O-$\beta''$. The refined lattice constant, order parameter $S$, the oxygen shift $\Delta z_O$ from $\beta'$ to $\beta''$, and temperature factors $U$ for SXRD and ND spectra are listed in Table II.

All of the model structures could be refined to an excellent agreement with the experimental data, where the values of weighted residuum $R_{wp}$ were as low as 4%. The values of the order parameter $S$ obtained from neutron refinements were considerably smaller than their SXRD counterparts, see Table II, although the conventional x-ray scans showed the ND and SXRD specimens should have a similar degree of ordering. The value of $S$ is derived from the refinement of structure factors. Neutron scattering is more sensitive to the local disorder in the material and this makes Rietveld refinement less accurate,[19] leading to high residua for the ND. Because the residua of structure factors $R_{F^2}$ for SXRD are an order of magnitude smaller than for ND (Table II), the order parameters $S$ from SXRD data should be more reliable and they also agree very well with the previous results, Fig. 1.

The Rietveld analysis confirms essentially complete order in PSW-PT for $x \leqslant 0.25$ and proves that the random site model is a correct description of the B chemistry in PSW-PT and PSW-PZ systems. The random site model is also the arrangement which maximizes the intensities of the superreflections because Sc has the lowest atomic number of all B cations. Since $F_{ord}=4(f_{\beta'}-f_{\beta''})$, the largest magnitude of $F_{ord}$ is achieved if the $\beta'$ site is occupied purely by Sc and all the remaining cations occupy $\beta''$. It is very unlikely that any other B-site structure could simulate equally well the observed strong intensities of the ordering reflections.

The large residuum $R_{F^2}$ of the refinements of the ND data was probably caused by many overlapping peaks in the high $Q$ range. While the high-$Q$ data seem to cause underestimates in $S$, they also allow much better accuracy for the temperature coefficients. A significant improvement in the fit was observed after the introduction of anisotropic temperature factors $U_{O11}$ and $U_{O33}$ for O (perpendicular and parallel to $\beta'$-O-$\beta''$) and separate values of $U_{\beta'}$ and $U_{\beta''}$ for the B sites. The refined temperature factors of Pb and O were very high, corresponding to unrealistically large magnitudes of

TABLE II. Results of Rietveld refinement of SXRD (x) and ND (n) data collected from PSW-PT and PSW-PZ at 290 K.

| $x$ | $a$ (Å) | $S$ | $\Delta z_O$ ($a$) | $U_{Pb}$ (Å$^2$) | $U_{O11}$ | $U_{O33}$ | $U_B$ | $R_{F^2}$ (%) | $R_{wp}$ (%) |
|---|---|---|---|---|---|---|---|---|---|
| 0 (x) | 8.1349 | 0.933 | 0.0054 | 0.055 | 0.034 | | 0.0039 | 6.7 | 4.0 |
| 0 (n) | 8.1360 | 0.847 | 0.0082 | 0.049 | 0.029 | 0.006 | 0.0054 | 40 | 4.5 |
| 0.15 Ti (x) | 8.1011 | 0.969 | 0.0075 | 0.043 | 0.017 | | 0.0033 | 9.7 | 3.7 |
| 0.15 Ti (n) | 8.0994 | 0.802 | 0.0080 | 0.048 | 0.023 | 0.005 | 0.0056 | 36 | 4.4 |
| 0.25 Ti (x) | 8.0761 | 0.948 | 0.0073 | 0.048 | 0.023 | | 0.0081 | 6.8 | 3.0 |
| 0.25 Ti (n) | 8.0785 | 0.644 | 0.0073 | 0.047 | 0.020 | 0.006 | 0.0056 | 36 | 4.3 |
| 0.35 Ti (x) | 8.0593 | 0.659 | 0.0069 | 0.050 | 0.039 | | 0.0110 | 8.0 | 3.6 |
| 0.35 Ti (n) | 8.0619 | 0.516 | 0.0038 | 0.047 | 0.022 | 0.009 | 0.0043 | 42 | 4.4 |
| 0.15 Zr (x) | 8.1615 | 0.760 | 0.0041 | 0.059 | 0.044 | | 0.0120 | 7.1 | 3.4 |
| 0.15 Zr (n) | 8.1644 | 0.589 | 0.0055 | 0.049 | 0.035 | 0.008 | 0.0055 | 42 | 4.7 |
| 0.35 Zr (x) | 8.1953 | 0 | | 0.051 | 0.045 | | 0.0090 | 6.9 | 2.5 |
| 0.35 Zr (n) | 8.2050 | 0 | | 0.053 | 0.043 | 0.009 | 0.0056 | 37 | 5.4 |

vibration of about 0.22 Å for Pb and 0.17 Å for O. Contrary to expectations, the temperature factors of Pb decreased after heating from 20 K to 290 K (e.g., from 0.052 $Å^2$ to 0.047 $Å^2$ for $x = 0.25$ Ti). These observations indicate that the large Debye-Waller factors are not due to temperature induced atomic vibrations, but rather are caused by local displacements of Pb and O atoms from their average lattice positions. The directions of these shifts are not correlated over larger distances, keeping the long-range structure cubic, but they are manifested through increased temperature factors. The increase in $U_{\mathrm{Pb}}$ at 20 K can be explained by the Pb shifts becoming more correlated at low temperatures. For the O atoms, the temperature factor $U_{\mathrm{O33}}$ along the B-O bond is 2–4 times smaller than the perpendicular component $U_{\mathrm{O11}}$. This suggests that the local O shifts occur mainly in the directions transverse to B-O, which could correspond to rotations of $BO_6$ octahedra. The temperature coefficients for the B cations have reasonable values and increase with temperature. All of the refined $\Delta z_{\mathrm{O}}$ were positive and indicated slight off-centering of oxygens away from the large Sc cation.

### B. Pair distribution function analysis

The PDF is obtained by calculating the inverse Fourier transformation of the entire diffraction spectrum, including the Bragg peaks and the intermediate diffuse intensities. Unlike the Rietveld method, PDF analysis makes no assumption about the periodicity of the investigated matter. The PDF provides information about the interatomic distances in the material, and has been extensively used to study glasses and liquids. The application of PDF analysis for crystalline materials is discussed elsewhere.[20–22] There are several equivalent forms of the PDF used in the literature. In this paper the PDF will always refer to the function $G(r)$, which is related to the local structure through

$$G(r) = \frac{1}{Nr\langle b\rangle^2} \sum_{i,j} [b_i b_j \delta(r - r_{ij})] - 4\pi r \rho_0,$$

where $b_i$, $b_j$ are the neutron-scattering lengths, $r_{ij}$ is the separation of the $i$th and $j$th atom, and $\rho_0$ is the number density of the material. Figure 5 shows the experimental PDF curves of PSW obtained by neutron scattering at 20 K and 290 K. The dotted line corresponds to the PDF calculated for the average, Rietveld structure, and the vertical grid indicates the expected interatomic distances. The experimental PDF's are markedly different from the calculated PDF; with additional peaks indicating that the local structure is significantly distorted from the average crystal lattice. The first peak of $G(r)$ at 2.1 Å is due to the B-O nearest neighbors, and its full width at half maximum is approximately 0.2 Å. This width is only slightly higher than the difference in the ionic radii of $Sc^{3+}$ and $W^{6+}$ ($\Delta R_\beta = 0.145$ Å, $r_{Sc^{3+}} = 0.745$ Å, $r_{W^{6+}} = 0.60$ Å), which indicates that B-cation off-center distortions are small. This conclusion is supported by the Rietveld analysis, which yielded small, realistic values for the Debye-Waller factors at the B sites (Table II), and it can be thus assumed that the B cations are close to their

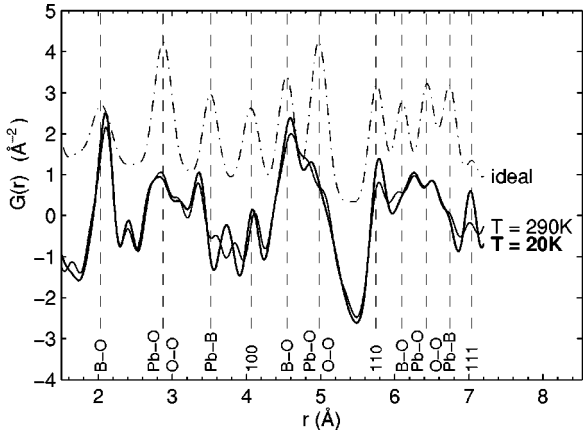


FIG. 5. PDF curves for PSW at 20 K, thick solid line, and at 290 K, thin line. Dash-dotted line denotes PDF calculated for the Rietveld-refined structure.

average positions. While the first peak roughly agrees with the calculated curve, there are significant deviations for the second and third peaks. The second nearest distance of Pb-O and O-O pairs is split into at least three overlapping peaks at 2.4 Å, 2.8 Å, and 3.1 Å. This splitting is unlikely to arise from the O-O bonds as a large distortion of the $BO_6$ octahedra would also affect the first B-O peak. As a result, there must be a large variance in the Pb-O bond lengths, which can be realized by shifts of the Pb cations or by rotations of the $BO_6$ octahedra. The presence of lead displacements is clearly confirmed by the third nearest-neighbor distance of Pb-B cations, which is separated into two peaks at about 3.4 Å and 3.7 Å. The $G(r)$ curves measured at 20 K and 290 K are quite similar overall, but they show a noticeable difference at $r \approx 3.5$ Å, corresponding to the Pb-B neighbors, see Fig. 5.

The Pb-B lengths are distributed among two peaks at 20 K, but with heating to 290 K they become more diffuse and form three maxima in the PDF. This can be attributed to cation oscillations in the local double-well potential or to a presence of a secondary distortion direction at the higher temperature. In either case, the correlation of Pb shifts appears to be disrupted. This is also supported by the decrease of peak amplitudes at $r \approx 5.75$ Å and $r \approx 7$ Å, corresponding to the $\langle 110\rangle$ and $\langle 111\rangle$ separations, respectively.

The PDF curves of $(1-x)$PSW–$(x)$PT, $x = 0$, 0.15, 0.25, 0.35, and $(1-x)$PSW–$(x)$PZ, $x = 0.15$, 0.35 are displayed in Fig. 6. The most apparent change in $G(r)$ of PSW-PT is the opposite amplitude trends for the B-O and Pb-B peaks at $r \approx 4.6$ Å and $r \approx 5.0$ Å. However, this is a compositional effect due to the negative scattering length of Ti. The impact of Ti is also noticeable on the first B-O peak, which becomes narrower with $x$ and develops a split at its left-side foot. Because of the negative value of $b_{\mathrm{Ti}}$, the Ti-O distance in the (0.65)PSW-(0.35)PT is represented by a local minimum at $r \approx 1.9$ Å. This minimum is offset from the main B-O peak by approximately 0.2 Å, close to the difference in the Sc and Ti radii ($\Delta R_\beta = 0.14$ Å, $r_{Sc^{3+}} = 0.745$ Å, $r_{Ti^{4+}} = 0.605$ Å). Thus it is not possible to determine without further modeling whether the increase in Ti composition induces larger shifts in the positions of the active W and Ti cations. Perhaps the

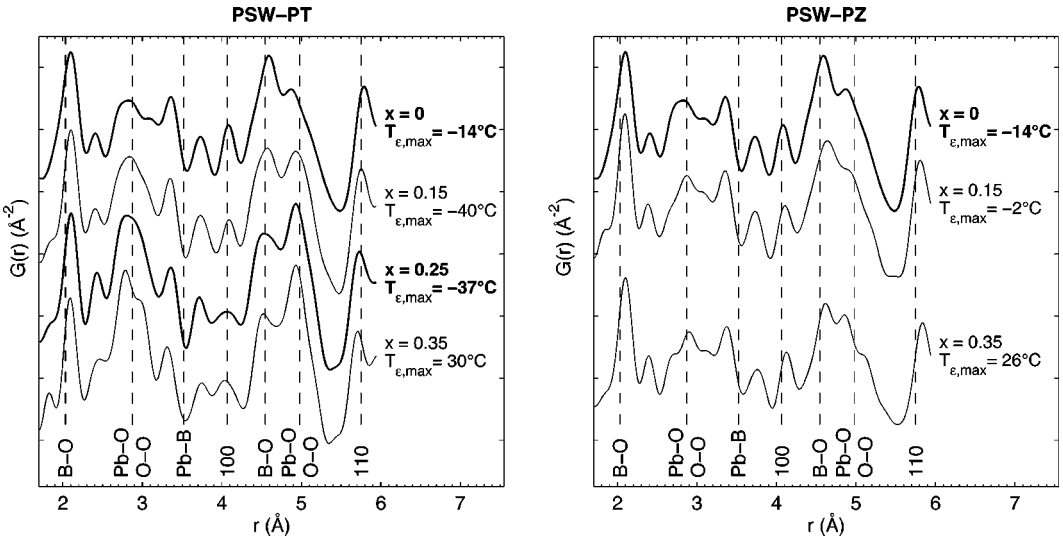


FIG. 6. PDF curves for PSW-PT and PSW-PZ at 20 K. Composition and $T_{\epsilon,\max}$ values are noted on the right side of plots.

most important feature in these PDF's is the evolution of the third peak at $r \approx 2.8$ Å, which is formed by Pb-O and O-O lengths. It has a right-side shoulder for PSW, then shows a very broad, diffuse profile for $x = 0.15$, 0.25 and redevelops a shoulder at $x = 0.35$. These alternations of the Pb-O peak coincide with the changes in the temperature of the permittivity maximum $T_{\epsilon,\max}$. The broad, diffuse Pb-O peak at $x = 0.15$, 0.25 suggests more randomness and a shorter correlation length of the Pb displacements, which seem to be consistent with the drop in $T_{\epsilon,\max}$. A similar trend can be observed in the PSW-PZ system, where the ''ruggedness'' of the main Pb-O peak grows with the substitution of Zr, and is accompanied by an increase in $T_{\epsilon,\max}$.

## IV. MODELING AND DISCUSSION

### A. Pair distribution function simulations

The real local structure of mixed-cation perovskites can be very complicated. With several cations at the B site many different local environments arise, inducing a variety of local shifts. As a result, the measured PDF is an average of many local arrangements. However, if there are dominant common patterns in the local arrangements it should be possible to reproduce the measured PDF by a relatively simple structural model. Several models of the local structure were examined and fitted to the experimental PDF's. The parameters of the structure models were fitted to minimize the residuum $R_w$ defined as

$$R_w = \sqrt{\frac{\sum_{k=1}^{N} w_k [G_{obs}(r_k) - G_{calc}(r_k)]^2}{\sum_{k=1}^{N} w_k G_{obs}^2(r_k)}}, \qquad (1)$$

where the weights $w_k$ showed only slight variation with $r$. The simulations were performed using the PDFFIT software, which employs the steepest descent minimization.[18] As the models became more complex with a larger number of parameters, this algorithm turned out to be inadequate, as it tended to converge to the nearest local minimum. The adopted solution was to perform Monte Carlo (MC) minimization on top of the PDFFIT results, i.e., the parameters obtained by PDFFIT were moved by MC and used in subsequent PDFFIT runs. This approach resulted in a significant improvement of the fit residua $R_w$ and also provided a statistical sample of refined parameters.

The models of the local structure were constructed using a $2 \times 2 \times 2$ cell with periodic boundary conditions, where the atomic occupancies, initial atomic coordinates, and Debye-Waller factors were taken from the results of the Rietveld analysis. All temperature coefficients were refined as isotropic, with separate factors for the Sc-rich $\beta'$, and mixed-cation $\beta''$, B sites. Several simple displacements of Pb and O atoms were examined, and their magnitudes, PDF scale factor, and temperature coefficients fitted to the experimental data.

In the first model, the Pb cations were allowed to shift along the [100], [110], [111] directions and in an antiparallel $\pm$[111] pattern from $\beta'$ to $\beta''$ sites. The oxygens could move along the B-O bond direction, changing the size of the $BO_6$ octahedra. The best fit for the 20 K data was always obtained using the first model with [100] Pb displacements, which reproduced the doubled peak for the Pb-B distances, Fig. 7(a). Because the average position of Pb is in the center of the $B_8$ cube, the shift in the [100] direction creates four short and four long Pb-B pairs, producing the experimentally observed double Pb-B peak. However, this model could not reproduce the Pb-O distances, in particular the shortest Pb-O length of 2.4 Å. Therefore, additional O displacements were introduced by allowing rotations of the $BO_6$ octahedra. General rotations of eight bound octahedra in the $2 \times 2 \times 2$ cell can be described by six parameters, e.g., by two rotation axes $r$, $s$ at [0 0 0] and [0.5 0.5 0.5], and their rotation angles. However, the refinement of all six parameters was numerically unstable, and the rotation axes had to be fixed in special directions. These were chosen as (i) $r = s = [10\bar{1}]$, (ii) $r = s$

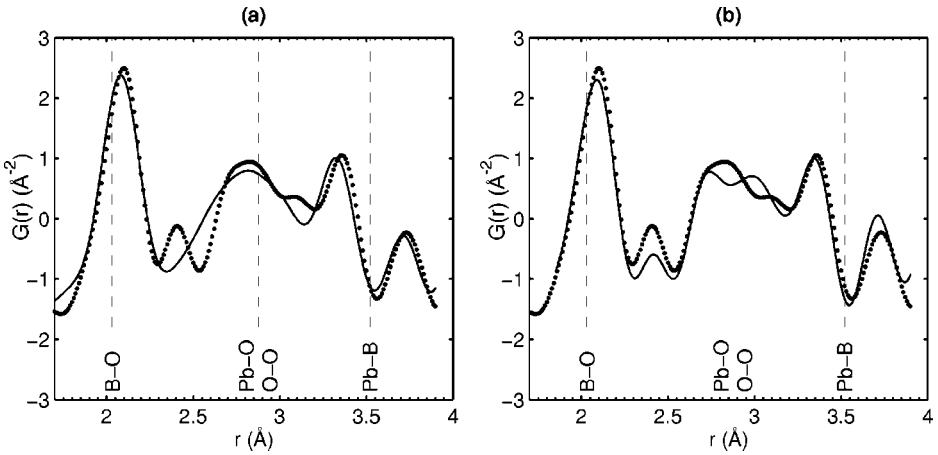


FIG. 7. Simulated (solid line) and measured (dots) PDF for PSW at 20 K. (a) common [001] Pb shifts, and (b) [001] Pb shifts with $BO_6$ rotations around $r=s=[10\bar{1}]$.

$=[\bar{2}11]$, and (iii) $r=[10\bar{1}]$, $s=[\bar{2}11]$. Type (i) rotation shifts four oxygens in the $O_{12}$ cage directly towards the central Pb, while the remaining eight oxygens move away. Rotation (ii) creates four shortened, four elongated and four unchanged Pb-O distances, and maximizes the difference between the shortest and longest Pb-O lengths, and the tilt (iii) is a combination of the previous types. These three tilt modes combined with [001] Pb shifts were tested for all $G(r)$ functions collected at 20 K. The best results were obtained using the type (i) rotation, especially in the shorter range of PDF at 1.7 Å$<r<$3.9 Å, as presented in Fig. 7(b). Although the $BO_6$ rotations resulted in a clear improvement of the fit and were able to reproduce the shortest Pb–O distance, the overall agreement with the Pb-O peak was far from perfect. In addition, when the refinement range was expanded to 8 Å, the rotation angles were considerably diminished and the agreement at short distances was lost. Displacements of the $\beta''$-site cations were investigated, but they failed to induce any appreciable change to the PDF. It appears that the real oxygen displacements are more complicated than those allowed by the constraints of $BO_6$ rotations. Such structures were simulated by allowing all oxygens to shift arbitrarily.

The free-oxygen simulations were performed with two modes of Pb displacements: in the [001] direction and in antiparallel $\pm[111]$ directions. The fit of $G(r)$ was carried out using the combined PDFFIT — Monte Carlo procedure. Both of the PDF models could be refined to perfect agreement with the experimental data, where the final residua were as low as $R_w=0.031$, see Fig. 8. Because of the high number of refined parameters (the maximum number of parameters meaningfully allowed is about 25 for this range[23,24]) it was essential to independently verify whether the resultant structures were chemical reasonable; this was done using the bond valence method.[25,26] The bond valence sums were calculated for all atoms in the simulated structure using the $R_{ij}$ parameters from Brese and Okeeffe.[25] The overall agreement of the forty valences in the unit cell was expressed as their standard deviation $R_{bvs}$ from the ideal valences:

$$R_{bvs}=\sqrt{\frac{1}{N}\sum_i (V_i-V_{i,ideal})^2}. \quad (2)$$

The respective valence deviations of the Pb [001] and Pb $\pm[111]$ models of (0.85)PSW-(0.15)PT were $R_{bvs}=0.415$ and $R_{bvs}=0.712$. These deviations are high in comparison with those obtained for Rietveld lattice ($R_{bvs}=0.226$), and the typical values in the models with $BO_6$ tilting ($R_{bvs}\approx 0.15$). The high $R_{bvs}$ values obtained for both free-oxygen models indicate that these local structures are unrealistic, despite the excellent agreement with experimental PDF.

The intermediate results of the MC minimization were recorded and contained many structures with low $R_w$ values, which could have improved valence agreement. To check their validity, the bond valence sums were calculated for ev-

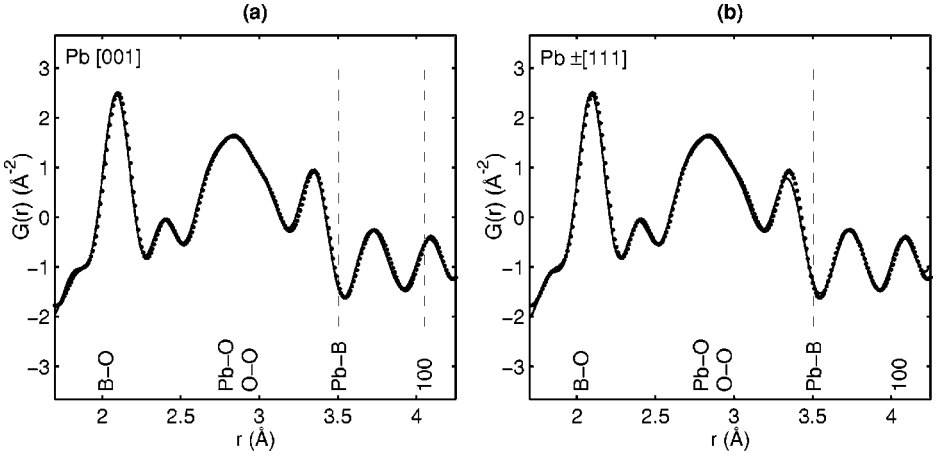


FIG. 8. PDF simulations for PSW-PT, $x=0.15$ at 20 K using free oxygen shifts with (a) [001] and (b) $\pm[111]$ Pb displacements.

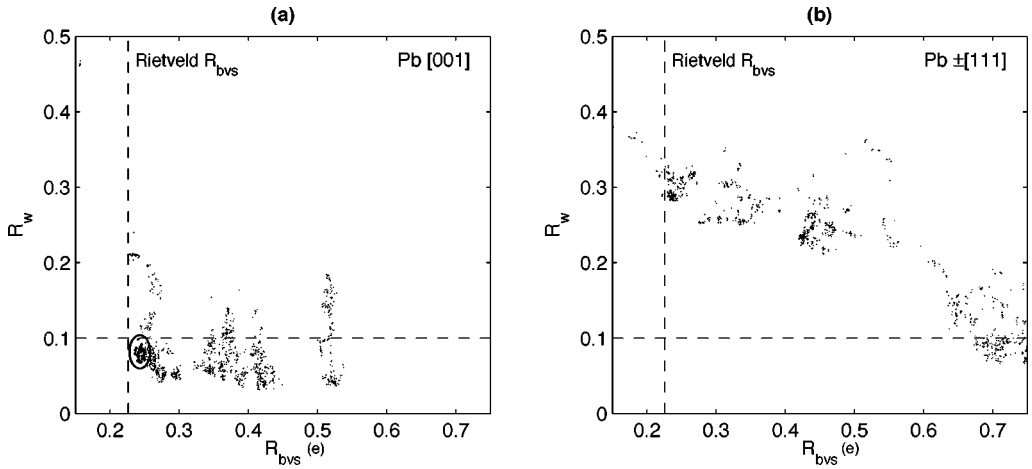


FIG. 9. Map of valence deviations $R_{bvs}$ vs fit residua $R_w$ for the MC PDF simulations of (0.65)PSW-(0.15)PT, Pb displacements are in (a) [001] and (b) $\pm$[111] directions. Low values of $R_w$ indicate good agreement with measured PDF; low values of $R_{bvs}$ indicate that the proposed structure is chemically reasonable. Horizontal and vertical dashed lines show the $R_w$ cutoff and the $R_{bvs}$ value of the Rietveld lattice, respectively. Points inside the oval in (a) were used to evaluate the lead polarizations.

ery step of the MC procedure. The structures were then evaluated based on the magnitude of valence deviation $R_{bvs}$ and a fit residuum $R_w$. This can be visualized by plotting a map of $R_{bvs}$ versus $R_w$ for all the MC steps. Figure 9 displays the $R_{bvs}$ maps for the two simulated modes of Pb displacements in PSW-PT with $x=0.15$. The map in Fig. 9(b) clearly indicates that structures with $\pm$[111] Pb shifts are not viable as all the structures with a low $R_w$ have very large $R_{bvs}$ and vice versa. However, for the [001] Pb shifts, Fig. 9(a), there are many structures with a low fit residuum ($R_w<0.1$), which also have acceptable $R_{bvs}$ values ($R_{bvs}<0.25$), close to the valence deviation of the Rietveld structure. The Pb polarization along [001], in spite of the overall polarization along [111], was also previously observed for PST.[13]

For each composition, fifty structures were chosen for further analysis by setting an $R_w$ cutoff (e.g., $R_w<0.1$ for PSW-PT with $x=0.15$) and selecting the structures with the lowest $R_{bvs}$ values. The selected structures are denoted by the enhanced points inside the oval in Fig. 9(a). The array of structures was then evaluated for common shift patterns. By examination of an ensemble of the local arrangements it is possible to gain better confidence in the results and probe the dispersion in the magnitudes and directions of the local shifts. The measured $G(r)$ corresponds to an average of many local arrangements present in the material. The investigation of an array of structures is thus a rough approximation of the real process of the PDF measurement.

A similar analysis of the fit residuum $R_w$ and valence agreement $R_{bvs}$, and the selection of ''good'' structures was also carried out for the remaining compositions of PSW-PT at 20 K. The O shifts along B-O were found to be about two times smaller than those in the perpendicular plane. Due to the unconstrained oxygen motion, the $O_{12}$ cage of the ideal A-site can be off-centered. Therefore, the Pb displacements should not be taken as absolute but need to be evaluated relative to the center of their $O_{12}$ environments. As a result, the shift directions can deviate considerably from the [001] direction. The polarization of the $PbO_{12}$ complexes were calculated for all of the selected structures. The obtained averages of the absolute and projected shift magnitudes, and the average scattering of polarization directions from the [001] direction, are listed in Table III. A typical standard deviation of the averaged displacement was about 0.004 Å. For the B-cation displacements, the attempted PDF simulations did not yield convincing results, possibly due to the strong signal from ferroelectrically inactive Sc atoms, which have the largest neutron-scattering length of the present atoms.

The magnitudes and angle scatter of directions of the $PbO_{12}$ polarizations exhibit qualitative correlation with the observed $T_{\epsilon,\max}$. As the Ti content is initially increased, the Pb displacements diminish and also become more scattered, Table III. For concentrations above $x=0.25$, the Pb displacements increase and angle scatter diminishes. This corresponds to the initial drop in $T_{\epsilon,\max}$ and the rise in $T_{\epsilon,\max}$, for $x\geqslant 0.25$. Larger Pb displacements with small scatter $\vartheta_{\mathrm{Pb}}$ are indicative of a deeper ferroelectric well, so based on the local structure changes an initial drop and subsequent rise in $T_{\epsilon,\max}$ are not surprising. The correlation is only qualitative since the Pb displacements are smaller for $x=0.25$ than for $x=0.15$, while the observed $T_{\epsilon,\max}$ is higher for $x=0.25$ than for $x=0.15$. Furthermore, if the dielectric response were

TABLE III. Results of the free-oxygen PDF simulations of PSW-PT at 20 K: $\overline{d}$, $\overline{d}_{001}$ are the average magnitude and the average [001] component of $Pb^{2+}$ polarization, $\vartheta_{\mathrm{Pb}}$ is its average deviation from [001], $\overline{R}_{bvs}$, $\overline{R}_w$ are the mean values of valence deviation and PDF fit residuum [Eqs. (1), (2)].

| $x$ | $\overline{d}$ (Å) | $\overline{d}_{001}$ (Å) | $\vartheta_{\mathrm{Pb}}$(°) | $\overline{R}_{bvs}$ | $\overline{R}_w$ | $T_{\epsilon,\max}$ (°C) |
|---|---|---|---|---|---|---|
| 0 | 0.381 | 0.379 | 4.4 | 0.24 | 0.058 | −14 |
| 0.15 | 0.375 | 0.372 | 5.8 | 0.24 | 0.079 | −40 |
| 0.25 | 0.321 | 0.309 | 16.5 | 0.26 | 0.090 | −37 |
| 0.35 | 0.330 | 0.323 | 11.2 | 0.34 | 0.116 | 30 |

TABLE IV. Local structure data and ferroelectric well depth obtained from DFT calculations for PSW-PT and PSW-PZ solid solutions. $d_{\mathrm{Pb}}$ is the average Pb atom displacement away from the center of its $O_{12}$ complex, $d_{\mathrm{W,Ti/Zr}}$ is the average W, Ti/Zr atom displacement away from the center of its $O_6$ complex, $\vartheta_{\mathrm{Pb}}$ is the angle scatter of Pb displacements, $R_{bvs}$ is the average valence deviation [Eq. (2)], and $\Delta E_{FE}$ is the depth of the off-center instability.

| $x$ | $d_{\mathrm{Pb}}$ (Å) | $d_{\mathrm{W,Ti/Zr}}$ (Å) | $\vartheta_{\mathrm{Pb}}$(°) | $R_{bvs}$ | $\Delta E_{FE}$(eV/cell) | $T_{\epsilon,\max}$ (°C) |
|---|---|---|---|---|---|---|
| 0 | 0.389 | 0.091 | 57 | 0.04 | −0.191 | −14 |
| 0.25 $Ti^{(ord)}$ | 0.361 | 0.095 | 30 | 0.05 | −0.141 | −37 |
| 0.25 $Ti^{(dis)}$ | 0.344 | 0.169 | 31 | 0.06 | −0.179 | 8 |
| 0.625 Ti | 0.350 | 0.201 | 24 | 0.07 | −0.137 | 244 |
| 1.0 Ti | 0.440 | 0.280 | 0 | 0.07 | −0.160 | 490 |
| 0 | 0.389 | 0.091 | 57 | 0.04 | −0.191 | −14 |
| 0.25 $Zr^{(dis)}$ | 0.390 | 0.105 | 30 | 0.06 | −0.235 | 13 |
| 0.625 Zr | 0.430 | 0.125 | 26 | 0.07 | −0.284 | 105 |

driven only by the Pb off-centering, the hardest ferroelectric response should be exhibited by PSW, as its simulation gave the largest and the most focused Pb displacements. However, $T_{\epsilon,\max}$ is significantly higher in the $x=0.35$ system, which suggests that the active $Ti^{4+}$ and $W^{6+}$ cations also contribute to the overall polarization. This is also supported by an increase in $T_{\epsilon,\max}$ in the disordered (0.75)PSW-(0.25)PT reported previously.[15]

Our analysis of the PDF's suggests that the initial drop in $T_{\epsilon,\max}$ is due to the changes in the Pb local environment with the substitution of the Ti ion into the ordered B-cation arrangement. Pb distortions become smaller, which indicates that the energy gain from Pb off-centering is diminished by Ti substitution. This leads to a decrease in $T_{\epsilon,\max}$. For Ti substitutions greater than $x=0.25$, formation of the Ti-O-Ti and W-O-Ti chains makes off-centering more favorable and leads to an increase in $T_{\epsilon,\max}$. To confirm the results of the PDF analysis for the Pb distortions and to probe the distortions of the B cations we used another technique, the first-principles density-functional theory calculations.

### B. Density-functional theory simulations of PSW-PT

The *ab initio* density-functional theory (DFT) simulations were performed for the PSW-PT and PSW-PZ systems using $2\times2\times2$ or $3\times2\times2$ supercells with periodic boundary conditions. The energy of the system was evaluated using a local-density approximation exchange-correlation functional[27] and was minimized with respect to the atomic coordinates by a quasi-Newton method[28] with no symmetry imposed. A $2\times2\times2$ $k$-point sampling of the Brillouin zone was used. The calculations were done with optimized norm conserving pseudopotentials.[29] Semicore states were included in the valence states of the pseudopotentials, and the designed nonlocal approach[30] was used to optimize pseudopotential transferability.[31]

Because the B-site stoichiometry must be commensurate with the cell dimensions, we were able to probe four PSW-PT compositions with $x=0$, 0.25, 0.625, and 1.0 and respective chemical formulas of $Pb_{12}[Sc_8W_4]O_{36}$, $Pb_8[Sc_4W_2Ti_2]O_{24}$, $Pb_8[Sc_2WTi_5]O_{24}$, and $Pb_8Ti_8O_{24}$. We also studied the PSW-PZ system at compositions of $x=0.25$ and 0.625. The (0.75)PSW-(0.25)PT composition was modeled in ordered and partially disordered configurations using B-site stoichiometries of $[Sc_4][W_2Ti_2]$ and $[Sc_3W][ScWTi_2]$, respectively. The disordered structure is not fully consistent with the compositions in Table I, however the occupancies of Sc correspond to an order parameter $S=0.5$. Both configurations were also used to model (0.75)PSW-(0.25)PZ. To compute the potential depth $\Delta E_{FE}$ related to the cation off-centering, the energies of the final structures were compared to the energies of the structures obtained by relaxing the oxygen atom coordinates while keeping the cations fixed at the high-symmetry positions. This yields structures with Pb and B cation still in the center of their oxygen complexes, but with relaxed B-O bond lengths.

The results of the calculations are presented in Table IV. For comparison, the bond valence sums were evaluated for the DFT structures and they display almost ideal values with $R_{bvs}<0.1$. The comparison of the DFT simulated structure of PSW with the experimental PDF at 20 K is presented in Fig. 10. Although the difference in the PDF curves is considerable, $R_w=0.34$, the peak positions in the calculated function agree well with the experimental data, and essentially all of the peaks are reproduced. Similar agreement was

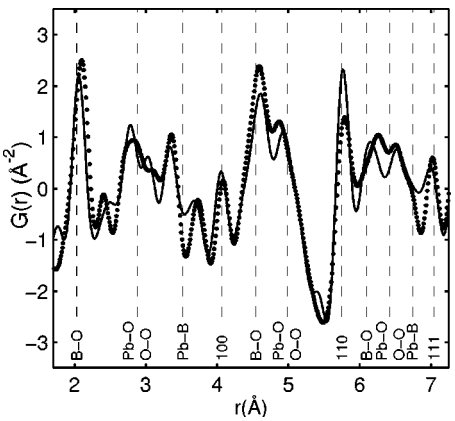


FIG. 10. PDF of DFT simulated structure of PSW (solid line) in comparison with the experimental data (dots).

obtained for all other compositions. The model structure of PSW had just one arrangement of the B cations which was periodically repeated. Many more local arrangements are possible in the real structure and their absence may account for the differences between the calculated and experimental curves. For the $Pb(Zr_{1-x}Ti_x)O_3$ solid solution, we have found that PDF's calculated from DFT-based simulations using large 320-atom supercells agreed closely with experimental data[32] and it is likely that calculations with large supercells will similarly improve agreement between the experimental and theoretical PDF's for the PSW-PT and PSW-PZ systems. The agreement between the experimental and DFT PDF's as well as the small deviations of the bond valence sums from their ideal values in the relaxed DFT structures, indicate that the structures obtained by DFT calculations are representative of the real local structure in PSW-PT and PSW-PZ.

The data in Table IV show that the magnitude of the ferroelectric instability $\Delta E_{FE}$ cannot be used to quantitatively predict changes in $T_{\epsilon,\max}$. For example, the $T_{\epsilon,\max}$ of $PbTiO_3$ (490 °C) is much higher than that of PSW (−14 °C) or (0.75)PSW-(0.25)PZ (10 °C), while the energy decrease from off-centering in $PbTiO_3$ is smaller (0.160 eV) than that of PSW (0.191 eV) and (0.75)PSW-(0.25)PZ (0.235 eV). Nevertheless, the instability magnitude exhibits qualitative agreement with the trends in $T_{\epsilon,\max}$ for the PSW-PT and PSW-PZ systems. In the PSW-PT, the depth of the off-center minimum first decreases from pure PSW to (0.75)PSW-(0.25)PT and then increases with further PT substitution. Disordering the B-cation arrangement in (0.75)PSW-(0.25)PT results in a sharply lowered $\Delta E_{FE}$, corresponding to the associated 45 °C rise in $T_{\epsilon,\max}$. In the PSW-PZ solid solution, PZ substitution results in a monotonic increase of the instability depth and correlates with the increase in $T_{\epsilon,\max}$.

The decrease in $T_{\epsilon,\max}$ from PSW to (0.75)PSW-(0.25)PT can be attributed to a decrease in perovskite volume, which has a large impact on the size of the off-centering instability.[33] Conversely, the increase in $T_{\epsilon,\max}$ from PSW to (0.75)PSW-(0.25)PZ is due to the increase in perovskite volume with the substitution of the large Zr cation. Despite the continuous decrease in volume with PT substitution in PSW-PT, the depth of the off-centering potential and $T_{\epsilon,\max}$ increase when PT content is greater than 0.25. This is due to the formation of the Ti-O-Ti chains as the Ti cations begin to populate both the $\beta'$ and $\beta''$ sites.

The transition temperature in PSW-PT and PSW-PZ show only a qualitative correspondence with the strengths of ferroelectric instabilities, because $T_{\epsilon,\max}$ is also determined by the relative energetics of other competing instabilities (e.g., rotational antiferrodistortive).[34,35] However, we find that changes in $T_{\epsilon,\max}$ for the PSW-PT and PSW-PZ solutions exhibit clear correlations with the cation shifts obtained from relaxed DFT structures, with an increased shift magnitude and smaller Pb angle scatter indicating a harder ferroelectric response and a higher $T_{\epsilon,\max}$. The addition of 25% Ti into PSW suppresses the magnitude and angle scatter of the Pb shifts due to a decrease in the perovskite volume; W and Ti shifts are essentially unchanged. The reduced Pb shift magnitudes are more important than the orientation of the Pb distortions, and $T_{\epsilon,\max}$ in (0.75)PSW-(0.25)PT is decreased. From $x=0.25$ to $x=0.625$, the Pb shifts decrease slightly and the Pb angle scatter is diminished, while the W and Ti shifts and the number of ferroelectric W and Ti cations rise dramatically. This leads to a large increase in $T_{\epsilon,\max}$. In pure $PbTiO_3$, the Pb and Ti shifts are large and the Pb angle scatter is eliminated, resulting in a very high $T_{\epsilon,\max}$. The increase in W and Ti shifts for $0.25<x<0.625$ arises from the formation of W-O-Ti and Ti-O-Ti chains. The effect of the formation of such chains can also be seen in disordered (0.75)PSW-(0.25)PT, which exhibits slightly smaller Pb shifts with the same angle scatter as the ordered system, but shows considerably increased (73%) W and Ti shifts, leading to a 45 °C rise in $T_{\epsilon,\max}$. In the PSW-PZ there is a small uniform increase in the Pb, W, and Zr shifts with increased Zr substitution, due to the expansion of the crystal by the addition of the large Zr ion. This leads to an essentially linear increase in $T_{\epsilon,\max}$.

The correlation between the cation shifts and $T_{\epsilon,\max}$ can be quantified by fitting the experimental values of $T_{\epsilon,\max}$ to a surprisingly simple function of the form

$$T_{\epsilon,\max} = a d_{\mathrm{Pb}}^2 + b d_{\mathrm{W,Ti/Zr}}^2 f_{\mathrm{W,Ti/Zr}} - 273, \tag{3}$$

where $d_{\mathrm{Pb}}$ is the average magnitude of the Pb shifts, $d_{\mathrm{W,Ti/Zr}}$ is the average magnitude of the W, Ti, and Zr shifts, $f_{\mathrm{W,Ti/Zr}}$ is the fraction of the W and Ti B cations in PSW-PT solution and W and Zr ions in PSW-PZ solution, $a$ and $b$ are constants in units of K/Å$^2$, and 273 converts from K to °C. This function is consistent with Abrahams-Kurtz-Jamieson (AKJ) relationship, which relates the square of the ferroelectric displacement to the Curie temperature.[36] The square of the displacement times the elastic module is proportional to the elastic energy due to ferroelectricity, and is thus directly related to the Curie temperature. While the AKJ relationship was proposed for the macroscopic lattice distortion, our results show that it applies to local distortions as well. The data in Table IV are well fit by

$$T_{\epsilon,\max} = 1704 d_{\mathrm{Pb}}^2 + 6080 d_{\mathrm{W,Ti/Zr}}^2 f_{\mathrm{W,Ti/Zr}} - 273. \tag{4}$$

The comparison of $T_{\epsilon,\max}$ values observed by experiment and obtained from Eq. (4) is presented in Fig. 11. The agreement between the two curves is quite good, especially for small substitutions of PT and PZ.

A rise or fall in $T_{\epsilon,\max}$ with composition is not directly caused by changes in the structural features such as the cation shifts, but is due to the changes in the energetics of the competing structural instabilities. However, in the case of PSW-PT and PSW-PZ solutions, the changes in local structure are excellent simple indicators of the shifts in the much more complicated energetic balance that gives rise to the changes in the $T_{\epsilon,\max}$. This may also be true for other ferroelectric solid solutions.

A comparison of the displacement data obtained by the PDF modeling and the DFT calculations (Tables III and IV) reveals several differences, e.g., different Pb scatter for PSW ($\vartheta_{\mathrm{Pb}}^{\mathrm{DFT}}=57°$, $\vartheta_{\mathrm{Pb}}^{\mathrm{PDF}}=4.4°$) and a much smaller increase of $d_{\mathrm{Pb}}$ for $x \geqslant 0.25$ in DFT calculations. Nevertheless, both

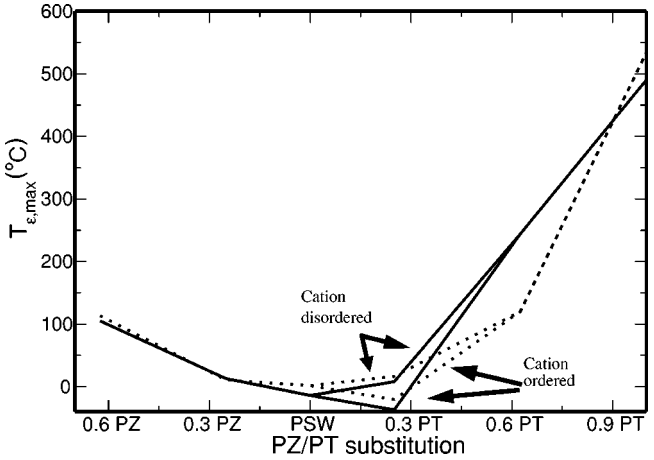


FIG. 11. Comparison of the $T_{\epsilon,\max}$ predicted by Eq. (4) (dashed) and experimentally observed $T_{\epsilon,\max}$ (solid) for PSW-PT and PSW-PZ solid solutions. The two sets of curves are for ordered and disordered PSW-PT.

methods give the same overall conclusion for the mechanism of the dielectric response in PSW-PT. In pure PSW the dominant effect for polarization is the lead off-centering. As Ti is added into the structure, the Pb displacements become smaller which leads to a decrease in $T_{\epsilon,\max}$. At first, the active Ti and W cations have little effect, since the high degree of B-site order confines them to distant $\beta''$ sites and they cannot form W-O-Ti or Ti-O-Ti linkages. However, for Ti concentrations with $x>0.25$ the Ti and W cations can occupy neighboring B-sites to produce increasingly large chains of active cations. At this point they dominate the dielectric response and reverse the trend in $T_{\epsilon,\max}$. Eventually, large ferroelectric domains with uniform Ti shifts are coupled with the Pb distortions, which become larger and more completely correlated.

Similar considerations can explain the uniform trend of $T_{\epsilon,\max}$ in the PSW-PZ system. In contrast to $Ti^{4+}$, the larger $Zr^{4+}$ ions increase the size of the unit cell, and the Pb distortions are not diminished. Second, as the B-site order is quickly destabilized in the PSW-PZ solution, there are no abrupt changes in the pattern of the B-site occupation. Finally, due to the large size difference, the clusters of Zr-O-W and Zr-O-Zr are unlikely to collaborate in a strong correlated ferroelectric distortion as is the case for the similarly sized W and Ti cations.

## V. CONCLUSIONS

By carrying out synchrotron x-ray and neutron-diffraction experiments, it was confirmed that the average structure of the PSW-PT and PSW-PZ systems at $x\leqslant 0.35$ is cubic with a random site arrangement of the B cations. There were no signs of rhombohedral or tetragonal peak splitting either at 20 K or at room temperature. The Rietveld analysis confirmed essentially complete B-site order in the solid solution of PSW-PT for $x\leqslant 0.25$. On the local scale the crystal lattice is considerably distorted from the average structure. This distortion is achieved through significant shifts of Pb and O atoms, while the B cations remain close to their average positions. The short-range experimental PDF's can be approximated by uniform Pb shifts in the [001] direction and bound rotations of $BO_6$ octahedra around the $[10\bar{1}]$ axis. The longer-range PDF is also consistent with the [001] Pb shifts, but more disordered O displacements are indicated. For an increased Ti content, the PDF simulations showed higher misorientation and reduced magnitude of the Pb shifts, which is consistent with the decline in $T_{\epsilon,\max}$. The DFT simulated structure of PSW displayed good agreement with the experimental PDF. The DFT results showed increased distortions of the active W and Ti cations for Ti concentrations $x>0.25$. Both PDF and DFT simulations indicate the unusual trend of $T_{\epsilon,\max}$ in PSW-PT is a combination of several effects. The initial decrease in $T_{\epsilon,\max}$ is due to reduced Pb displacements, which are caused by the decreasing unit cell volume. At the same time, the high B-site order keeps W and Ti cations separated by the ferroelectrically inactive Sc ions. However, as the ordering is disrupted at $x>0.25$, Ti and W can couple their polarizations through the formation of Ti-O-W or Ti-O-Ti chains, and dominate the dielectric response. In contrast, the substitution of $Zr^{4+}$ increases the cell volume and rapidly reduces the B-site order; as a result, the PSW-PZ system shows a simple, linear change in $T_{\epsilon,\max}$.

## ACKNOWLEDGMENTS

The authors are grateful to Dr. Beatriz Noheda from the National Synchrotron Light Source (NSLS), Brookhaven National Lab and Dr. Simine Short from Intense Pulse Neutron Source (IPNS), Argonne Lab for help with the experiments. The NSLS was supported by the Department of Energy, Division of Materials Sciences and of Chemical Sciences. The IPNS was supported by the US Department of Energy, Division of Materials Science. Computational support was provided by the High-Performance Computing Modernization Office of the Department of Defense. This work was funded by the Office of Naval Research Grants Nos. N00014-01-1-0860 and N00014-01-1-0372, the Center for Piezoelectrics by Design and the NSF MRSEC Program, under Grant No. DMR00-79909. A.M.R. would also like to thank the Camille and Henry Dreyfus Foundation for support.

*Electronic address: juhas@pa.msu.edu
†Electronic address: davies@lrsm.upenn.edu

[1] M.A. Akbas and P.K. Davies, J. Am. Ceram. Soc. **80**, 2933 (1997).
[2] Y. Yan, S.J. Pennycook, Z. Xu, and D. Viehland, Appl. Phys. Lett. **72**, 3145 (1998).
[3] P.K. Davies and M.A. Akbas, Ferroelectrics **221**, 27 (1999).
[4] W. Dmowski, M.A. Akbas, T. Egami, and P.K. Davies, J. Phys. Chem. Solids **63**, 15 (2002).
[5] C. Malibert, B. Dkhil, J.M. Kiat, D. Durand, J.F. Berar, and A. Spasojevic-de Bire, J. Phys.: Condens. Matter **9**, 7485 (1997).
[6] O. Bidault, C. Perrin, C. Caranoni, and N. Menguy, J. Appl. Phys. **90**, 4115 (2001).
[7] C. Perrin, N. Menguy, O. Bidault, C.Y. Zahra, A.-M. Zahra, C.

Caranoni, B. Hilczer, and A. Stepanov, J. Phys.: Condens. Matter **13**, 10 231 (2001).
[8] F. Chu, N. Setter, and A.K. Tagantsev, J. Appl. Phys. **74**, 5129 (1993).
[9] N. Setter and L.E. Cross, J. Appl. Phys. **51**, 4356 (1980).
[10] C.G.F. Stenger and A.J. Burggraaf, Phys. Status Solidi A **61**, 653 (1980).
[11] S. Teslic and T. Egami, Acta Crystallogr., Sect. B: Struct. Sci. **54**, 750 (1998).
[12] J.M. Kiat, G. Baldinozzi, M. Dunlop, C. Malibert, B. Dkhil, C. Menoret, O. Masson, and M.T. Fernandez-Diaz, J. Phys.: Condens. Matter **12**, 8411 (2000).
[13] W. Dmowski, M.A. Akbas, P.K. Davies, and T. Egami, J. Phys. Chem. Solids **61**, 229 (2000).
[14] G. Shirane, R. Pepinsky, and B.C. Frazer, Acta Crystallogr. **9**, 131 (1956).
[15] P. Juhas, P.K. Davies, and M.A. Akbas, in Fundamental Physics of Ferroelectrics 2002, edited by Ronald E. Cohen, AIP Conf. Proc. 626 (AIP, Melville, NY, 2002), pp. 108–116.
[16] A.C. Larson and R.B. von Dreele, GSAS, Los Alamos National Laboratory Report No. LAUR 86-748 (2000) (unpublished).
[17] P.F. Peterson, M. Gutmann, T. Proffen, and S.J.L. Billinge, J. Appl. Crystallogr. **33**, 1192 (2000).
[18] T. Proffen and S.J.L. Billinge, J. Appl. Crystallogr. **32**, 572 (1999).
[19] W. Dmowski, T. Egami, L. Farber, and P.K. Davies, in Fundamental Physics of Ferroelectrics 2001, edited by Henry Krakaur, AIP Conf. Proc. 582 (AIP, Melville, NY, 2001), pp. 33–44.
[20] T. Egami, Mater. Trans., JIM **31**, 163 (1990).
[21] B.H. Toby and T. Egami, Acta Crystallogr., Sect. A: Found. Crystallogr. **A48**, 336 (1992).
[22] S.J.L. Billinge, Ph.D. thesis, University of Pennsylvania, 1992.
[23] T. Egami and S.J.L. Billinge, *Underneath the Bragg Peaks: Structural Analysis of Complex Materials* (Pergamon, Elsevier, Oxford, England, 2003).
[24] *Local Structure from Diffraction*, edited by S.J.L. Billinge and M.F. Thorpe (Plenum Press, New York, 1998).
[25] N.E. Brese and M. Okeeffe, Acta Crystallogr., Sect. B: Struct. Sci. **47**, 192 (1991).
[26] I.D. Brown and D. Altermatt, Acta Crystallogr., Sect. B: Struct. Sci. **41**, 244 (1985).
[27] J.P. Perdew and A. Zunger, Phys. Rev. B **23**, 5048 (1981).
[28] B.G. Pfrommer, M. Cote, S.G. Louie, and M.L. Cohen, J. Comput. Phys. **131**, 233 (1997).
[29] A.M. Rappe, K.M. Rabe, E. Kaxiras, and J.D. Joannopoulos, Phys. Rev. B **41**, 1227 (1990).
[30] N.J. Ramer and A.M. Rappe, Phys. Rev. B **59**, 12 471 (1999).
[31] I. Grinberg, N.J. Ramer, and A.M. Rappe, Phys. Rev. B **63**, 201102 (2001).
[32] I. Grinberg, V.R. Cooper, and A.M. Rappe, Nature (London) **419**, 909 (2002).
[33] R.E. Cohen, Nature (London) **358**, 136 (1992).
[34] M. Fornari and D.J. Singh, Phys. Rev. B **63**, 092101 (2001).
[35] J. Iniguez, D. Vanderbilt, and L. Bellaiche, Phys. Rev. B **67**, 224107 (2003).
[36] S.C. Abrahams, S.K. Kurtz, and P.B. Jamieson, Phys. Rev. **172**, 551 (1968).